Design and Use of Tailored Hard-Pulse Trains for Uniformed Saturation of Myocardium at 3 Tesla

Kyunghyun Sung* and Krishna S. Nayak

Complete and uniform saturation of myocardium is essential for quantitative myocardial perfusion imaging using the first pass of a contrast agent. At 3 T, inhomogeneities of both the static (B_0) and radiofrequency (B_1) magnetic fields have led to the use of adiabatic B_1-insensitive rotation type 4 (BIR-4) pulses, which in practice are constrained by radiofrequency (RF) heating. In this study, we propose the use of trains of weighted hard pulses that are optimized for the measured variation of B_0 and B_1 fields in the myocardium. These pulses are simple to design, and require substantially lower RF power when compared with BIR-4 pulses. In volunteers, at 3 T, we demonstrated that the proposed saturation pulse with three subpulses results in lower peak and lower average residual longitudinal magnetization over the heart, as compared with 8-msec BIR-4 pulses and conventional hard pulse trains ($P < 0.05$). Magn Reson Med 60:997–1002, 2008. © 2008 Wiley-Liss, Inc.

Key words: RF saturation pulses; B_1 inhomogeneity; cardiac MRI; myocardial perfusion imaging

First-pass magnetic resonance (MR) myocardial perfusion imaging (MPI) is an established technique for the assessment of ischemic heart disease (1–3). Saturation recovery preparation is widely used to produce T_1-weighted images rapidly and with multiple slice coverage. Contrast-to-noise ratio (CNR) of myocardial wall enhancement during the first pass is critical to the performance of this technique. Recent work at 3 T has demonstrated improved CNR and showed that the diagnostic performance of 3-T MPI is superior to that of 1.5 T for the identification of both single- and multiple-vessel coronary disease (4). Despite the gain in CNR, there are still major technical challenges in 3-T cardiac imaging, such as static (B_0) and radiofrequency (B_1) magnetic field inhomogeneities (5–9).

Qualitative and quantitative MPI both rely on complete and uniform saturation of myocardium, and the performance of saturation pulses is sensitive to variations in the B_0 and B_1 fields. Recent studies have compared the effectiveness of different saturation pulses and have shown that the rectangular RF pulse train (10) and the adiabatic B_1-insensitive rotation type 4 (BIR-4) pulse (11) exhibit better saturation effectiveness than the conventional 90° rectangular hard pulse with 1.5-T and 3-T cardiac imaging (12–15). However, the conventional RF pulse train is more susceptible to B_1 inhomogeneity than the BIR-4 pulse. Conversely, the BIR-4 pulse has a higher specific absorption rate (SAR). These costs inherently limit their application at 3 T, where low RF power deposition and immunity to B_0- and B_1-field inhomogeneities are highly desirable.

In this work, we hypothesize that tailored pulse train designs, based on estimated B_0 and B_1 profiles that were measured a priori over the heart, can overcome both SAR and B_1 inhomogeneity constraints. Compared with the conventional 90° pulse train, the tailored pulse train consists of hard pulses with unequal weighting. The tailored-pulse-train design is considered to improve the immunity to B_1 variation (16), while maintaining low RF power. In this study, the performance of the proposed tailored pulse train is tested using simulations and in vivo experiments at 3 T.

METHODS

Experimental Methods

Experiments were performed on a commercial whole-body 3.0-T scanner (Signa Excite HD; GE Healthcare, Waukesha, WI) with gradients capable of 40-mT/m amplitude and 150-T/m/sec slew rate. A body coil was used for RF transmission and an 8-channel phased-array cardiac coil was used for signal reception. Parallel imaging was not used. In all studies, the transmit gain was calibrated using a standard pre-scan and the center frequency was adjusted over a three-dimensional (3D) region of interest containing the left ventricle (LV). Synchronization with the cardiac cycle was achieved with prospective triggering based on an electrocardiogram (ECG) signal. The institutional review board of the University of Southern California approved the imaging protocols. Each subject was screened for magnetic resonance imaging risk factors and provided informed consent in accordance with institutional policy.

Measurement of B_0 and B_1 Variation

B_0 and B_1 maps were measured in 8 healthy subjects (1 female and 7 males, age 29 ± 4.7 years, height 177 ± 5.8 cm, weight 70 ± 7.1 kg) with 6–8 parallel short-axis slices (6 subjects) and 1 short-axis slice (2 subjects). Cardiac B_0 maps were obtained in a single breath-hold using cardiac-gated gradient-echo sequences with two echo times (TEs). Signal from fat was reduced using a fat-saturation prepulse. Imaging parameters were: field of view (FOV) = 30 cm; in-plane resolution = 2.6 mm, TE = 1.6 msec and 3.6 msec (±250-Hz frequency range); repetition time (TR) = 12.8 ms; flip angle = 30°; and slice thickness = 5 mm.

Cardiac B_1 maps were acquired in a single breath-hold using the cardiac gated saturated double-angle method (SDAM), as previously described (9,17,18). The transmit

Magnetic Resonance Engineering Laboratory, Ming Hsieh Department of Electrical Engineering, University of Southern California, Los Angeles, California, USA.

Grant sponsor: American Heart Association; Grant number: 0435249N; Grant sponsor: James H. Zumberge Foundation.

*Correspondence to: Kyunghyun Sung, University of Southern California, 3740 McClintock Avenue, EEB 412, Los Angeles, CA 90089-2564. E-mail: kyunghsu@sipi.usc.edu

Received 16 March 2008; revised 27 May 2008; accepted 26 June 2008.
DOI 10.1002/mrm.21765
Published online in Wiley InterScience (www.interscience.wiley.com).

gain was calibrated for each individual subject. The B_1 scale was computed as the measured flip angle divided by the prescribed flip angle. Imaging parameters were: FOV = 30 cm; in-plane resolution = 5 mm; TE = 2 msec; TR = 7.2 msec; prescribed flip angle = 60° and 120°; and slice thickness = 5 mm.

The LV myocardium was manually segmented in each image, and a composite 2D histogram was produced in B_0–B_1 space. A region of interest (ROI) was defined that contained B_0 and B_1 values representative of nearly all myocardial pixels from all subjects and all imaging slices. This ROI was used for subsequent tailored-pulse-train optimization.

Optimization of Pulse Trains

Weighted hard-pulse trains (α_1,..., α_n) of length n were designed to minimize the maximum residual longitudinal magnetization (M_z) over the B_0–B_1 ROI. An exhaustive search based on numerical Bloch simulations was performed with the following cost function:

$$C = \max_{\text{ROI}} \left| \frac{M_z}{M_0} \right|. \quad [1]$$

Each α_i ranged from 70° to 240° in steps of 1° for $n \leq 3$, and 5° for otherwise ($4 \leq n \leq 6$). Minimum and maximum α_i constraints were determined by 90° divided by the minimum and maximum B_1 scale of the ROI. The peak B_1 amplitude was fixed at 0.115G, a typical value of body-coil transmission in commercial scanners when imaging medium to large-sized humans. We ignored T_1 relaxation between RF subpulses, and assumed the residual transverse magnetization was completely removed by the crusher gradients. Therefore, the subpulses in a set (α_1,..., α_n) had no specific order, reducing the computation time.

In Vivo Pulse Performance

In vivo tests of the proposed method were performed in 4 healthy volunteers (1 female and 3 males, age 31 ± 2.1 years, height 173 ± 5.3 cm, weight 67 ± 8.1 kg) with three cardiac views (axial, short-axis, and four-chamber). The tailored pulse train with $n = 3$ was compared with an 8-ms BIR-4 pulse with tanh/tan (amplitude/frequency) modulation functions ($\beta = 5$ and $\tan(\kappa) = 80$) (11), and conventional pulse train using a saturation-no-recovery (SR) experiment, as previously described (12,13). Identical transmit gain and shim values were maintained during the comparison. A 2DFT fast gradient echo (FGRE) acquisition with a center-out k-space trajectory was used with a 10° flip angle. Proton-density (PD) weighted images with a 3° flip angle were also acquired in the same breath-hold for normalization. The pulse sequence was cardiac-gated and there was one heartbeat between SR and PD acquisition to allow full recovery of magnetization, resulting in a single breath-hold of 5 heartbeats (2 for SR images, 1 for recovery, and 2 for PD images). Each saturation pulse (BIR-4, pulse train, and tailored pulse train) was employed in the FGRE pulse sequence, and acquired in a separate breath-hold. Imaging parameters were: FOV = 30 cm; TE = 1.2 msec; TR = 3.4 msec, acquisition matrix = 64 × 64; in-plane resolution = 4.7 mm; slice thickness = 5 mm; image acquisition time = 109 msec; and bandwidth = ±125 kHz.

For image analysis, the SR images were normalized by the PD images (SR/PD) to remove the effect of receive coil sensitivity and other system imperfections, and then multiplied by sin3°/sin10° to compensate for the excitation angle difference. The resulting images reflect $|M_z/M_0|$ and have a range from 0 (complete saturation) to 1 (no saturation). LV and right ventricle (RV) were manually defined based on the PD images. We computed the maximum and average $|M_z/M_0|$ over the LV and LV+RV, and report mean ± SD. All image analysis and numerical simulations were performed in MATLAB, version 7.0 (The Mathworks, Inc., Natick, MA).

RESULTS

Measurements of B_0 and B_1 Variation

Fig. 1a (top) illustrates the measured B_0 and B_1 maps from a mid-short-axis slice in one representative volunteer. A Gaussian mixture model (GMM) was initially applied to cluster a region by using the expectation maximization algorithm to estimate the order and parameters of the GMM (19). The 2D histogram of a given B_0–B_1 set and its clustered region (red line) are shown in Fig. 1a (bottom).

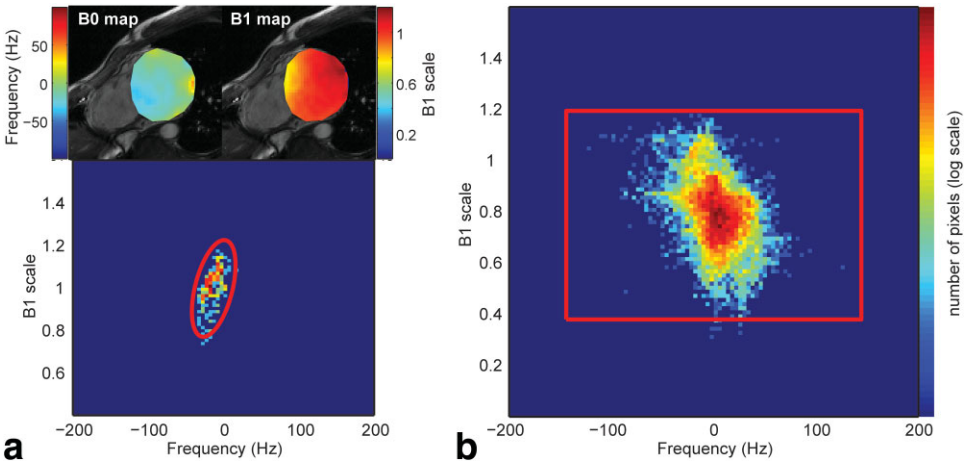

FIG. 1. Measured B_0 and B_1 inhomogeneity over the left ventricle at 3 T: **(a)** B_0 and B_1 maps from a single slice for 1 subject; and **(b)** the combined 2D histogram from all slices for all 8 subjects. The extent of the B_0–B_1 ROI (red rectangle) was based on the extent of the B_0–B_1 clusters (red oval) computed using Gaussian mixture models for each slice in each subject. The ROI contains 99.7% of all scattered pixels. [Color figure can be viewed in the online issue, which is available at www.interscience.wiley.com.]

Table 1
Prescribed Flip Angles, Max $|M_z/M_0|$, and Relative RF Power for Optimized Tailored Pulse Trains

n	Optimal weighting						Max $\|M_z/M_0\|$	Relative RF power[a]
1	114°						0.737	1.3
2	116°	231°					0.268	3.9
3	96°	228°	141°				0.087	5.2
4	120°	90°	180°	230°			0.043	6.9
5	90°	110°	145°	205°	235°		0.016	8.7
6	90°	170°	130°	105°	220°	240°	0.007	10.6

[a]Relative RF energy is defined as the pulse RF energy divided by the RF energy of a single 90° hard pulse (duration 0.5 ms). All pulses use a peak B1 amplitude of 0.115G.

We then chose a rectangular B_0–B_1 ROI to represent the expected B_0–B_1 variation based on the GMM clustered regions, and minimum and maximum B_0–B_1 values. Fig. 1b shows a 2D histogram of all 8 subjects and its corresponding rectangular ROI. The ROI overestimates the inhomogeneities of B_0–B_1 fields to consider all possible cases, and contains 99.7% of all scattered data points. The ROI spans resonance offsets of –144 Hz to +144 Hz, which is in good agreement with the range reported in the literature (5), and a B_1 scaling range of 0.38–1.2, which contains the range obtained in a previous study (0.45–1.12) (9).

Simulated Pulse Performance

The pulse train weighting was optimized to produce the minimum cost according to Eq. [1]. Table 1 contains the optimal flip angles for n = 1–6, and the corresponding max $|M_z/M_0|$ and relative RF energies. The relative RF energy was calculated as the RF energy of a pulse train divided by the RF energy of a single 90° hard pulse (duration 0.5 msec). Fig. 2 plots the residual M_z/M_0 and the RF energy as a function of n in simulation. The maximum values of $|M_z/M_0|$ within the ROI for the tailored pulse train were compared with those for the BIR-4 and pulse train. Because the rectangular ROI overestimates the actual behavior of B_0–B_1 inhomogeneity for each subject, we also computed the average $|M_z/M_0|$ value and the standard deviation (SD) of M_z/M_0 over the ROI. The tailored-pulse-train designs showed superior saturation performance compared with the conventional pulse train, with only a small increment in the relative RF energy.

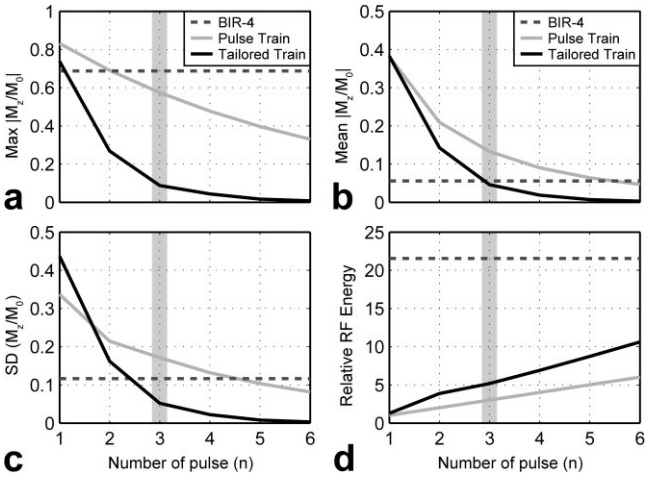

FIG. 2. Behavior of residual M_z and the corresponding RF energy as a function of n. **(a)** Max $|M_z/M_0|$, **(b)** mean $|M_z/M_0|$, **(c)** SD of M_z/M_0, and **(d)** relative RF energy were simulated for the BIR-4 pulse (dotted line), conventional pulse train (gray line), and tailored pulse train (black line). The tailored pulse train when $n \geq 3$ shows superior saturation performance than the BIR-4 and pulse train while maintaining lower relative RF energy than the BIR-4 pulse.

When n = 3, the behavior of the residual M_z/M_0 (max $|M_z/M_0|$, mean $|M_z/M_0|$, and SD M_z/M_0) for the tailored pulse train indicates better saturation performance compared with the BIR-4 pulse, while maintaining lower relative RF energy. Fig. 3a–c shows pulse sequence diagrams for the three different saturation pulses considered in this study. The tailored pulse train (n = 3) had a 7.7-msec pulse duration (Fig. 3c). The optimal pulse weighting was 96°, 228°, and 141° (0.548, 1.296, and 0.804 msec, respectively), and the order was chosen among all the six possible combinations by including T_1 relaxation (T_1 = 1115 msec) in the cost function. The spoiler gradients (1 ms) and crusher gradients (3 msec–2 msec–2 msec) were cycled to avoid stimulated echoes, as previously described (10,13,14). The tailored pulse train produced 4.2 times lower relative RF energy than the BIR-4 pulse, and 1.7 times higher relative RF energy than the pulse train.

Fig. 3d–f shows the saturation profiles as a function of off-resonance (horizontal axis) and B_1 scale (vertical axis) using numerical Bloch simulation for the three saturation pulses. The ROI used for optimization is shown in red. The profile for the BIR-4 pulse (Fig. 3d) had excellent saturation for most of the B_1 range, but its B_0 bandwidth became less than ±110 Hz as the B_1 scale fell below 0.43. This can be problematic when both the B_0 and B_1 fields are severely distorted. The conventional pulse train (Fig. 3e) showed excellent B_0 variation insensitivity due to its effective bandwidth of ±1000 Hz, but the peak M_z/M_0 became larger than 0.1 when the B_1 scale was smaller than 0.7. This explains the weaker B_1 immunity of the pulse train, as previously discussed. The tailored pulse train with the optimal weighting (Fig. 3f), however, improved the saturation performance, and produced excellent saturation effectiveness over the entire ROI.

In Vivo Pulse Performance

Fig. 4 shows representative normalized SR images with the different saturation pulses in three cardiac views. Cardiac cine images (left column) are displayed to provide an anatomical reference. Table 2 summarizes the saturation

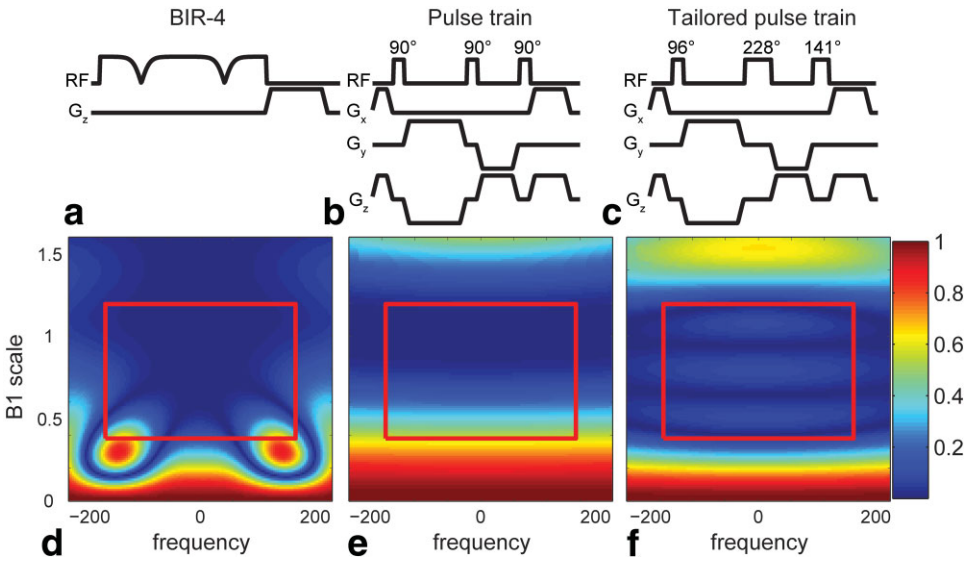

FIG. 3. Saturation pulse sequence diagrams for **(a)** the BIR-4, **(b)** conventional pulse train, and **(c)** tailored pulse train ($n = 3$), and corresponding simulated $|M_z/M_0|$ profiles **(d–f)**. The B_0–B_1 ROI is indicated by the red box. The simulation profile for the tailored pulse train **(f)** shows reduced peak $|M_z/M_0|$ within the ROI. [Color figure can be viewed in the online issue, which is available at www.interscience.wiley.com.]

effectiveness for the different saturation pulses. Both the BIR-4 and tailored pulse showed comparable saturation performance over the LV, whereas the conventional pulse train became less effective in septal myocardium. The peak and average residual $|M_z/M_0|$ over the LV for the tailored pulse train were smaller than those for the BIR-4 and conventional pulse train, but only the peak value was significantly different ($P < 0.05$). The residual $|M_z/M_0|$ within the LV+RV behaved differently, and the BIR-4 pulse demonstrated inferior performance compared with the tailored pulse train. The peak and average residual $|M_z/M_0|$ over the LV+RV for the tailored pulse train were significantly smaller than those for the BIR-4 and conventional pulse train ($P < 0.05$). Note that the measured values were influenced by low SNR and T_1 recovery during the acquisition, and therefore could not represent the absolute saturation effectiveness.

DISCUSSION

The proposed modification of RF pulse trains was implemented to increase immunity to B_0 and B_1 variation. We demonstrated the train of tailored hard RF pulses to have superior saturation effectiveness in simulation and in vivo, with the cost of 1.7-times-higher RF power than the conventional 90° pulse train. Compared with the BIR-4 pulse, the tailored pulse showed superior saturation over the heart while requiring 4.2 times less RF power. This alleviates the SAR constraints and should enable more frequent use of saturation pulses or more extensive coverage of the myocardium in 3-T MPI (e.g., more slices per heartbeat).

We confined the total number of subpulses to three in this validation study, because three subpulses were the minimum number that was predicted to produce satura-

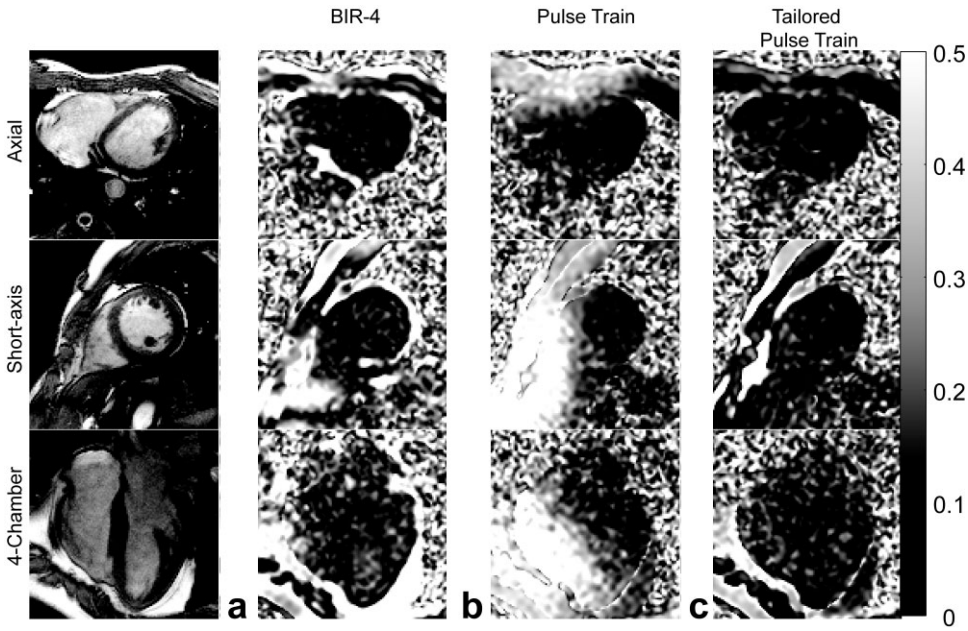

FIG. 4. Representative normalized SR images with the **(a)** BIR-4, **(b)** conventional pulse train, and **(c)** tailored pulse train in three cardiac views. The proposed saturation pulse demonstrates better saturation performance over the LV and RV than the BIR-4 and pulse train.

Table 2
In Vivo Performance of Myocardial Saturation Pulses at 3 Tesla

	RF Pulse duration	Relative RF power	LV		LV and RV	
			Max $\lvert M_z/M_0\rvert$	Mean $\lvert M_z/M_0\rvert$	Max $\lvert M_z/M_0\rvert$	Mean $\lvert M_z/M_0\rvert$
BIR-4	8.0 msec	21.6	0.28 ± 0.066	0.11 ± 0.022	0.57 ± 0.259	0.14 ± 0.046
Conventional pulse train	6.5 msec	3	0.32 ± 0.133	0.12 ± 0.055	0.81 ± 0.335	0.21 ± 0.093
Tailored pulse train	7.7 msec	5.2	0.22 ± 0.062	0.09 ± 0.017	0.26 ± 0.086	0.097 ± 0.019

tion performance superior to both the conventional pulse train and BIR-4. Tailored pulse trains with more than three subpulses may improve the saturation performance (max $\lvert M_z/M_0\rvert$ and mean $\lvert M_z/M_0\rvert$) with a small increment in RF power and pulse duration, as shown in Table 1. It should be noted that BIR-4 pulses can also be optimized based on B_0–B_1 maps—for example, when choosing amplitude and frequency modulation functions. Fig. 5 shows the mean $\lvert M_z/M_0\rvert$ as a function of β and tan(κ) with a fixed RF pulse duration (8 msec). This simulation suggests that an optimized BIR-4 pulse can reduce average residual M_z by 4.3% while increasing RF power by 8.3%.

Paramagnetic contrast agents during the first pass, and stents, sternal wire, and other metal implants can potentially create additional B_0 inhomogeneity due to increased susceptibility effects (20), widening the B_0–B_1 ROI. The tailored pulse train consists of RF pulses with different bandwidths, and has an effective B_0 bandwidth of ±390 Hz. Therefore, the additional off-resonance caused by the contrast agents is not expected to degrade the saturation performance of the tailored pulse. However, the saturation performance of the BIR-4 pulse, due to its limited bandwidth, can be impacted. The effective bandwidth in the tailored pulse train can be increased by either lowering the maximum α_i constraint in the cost function or increasing the peak B_1 amplitude in the pulse design.

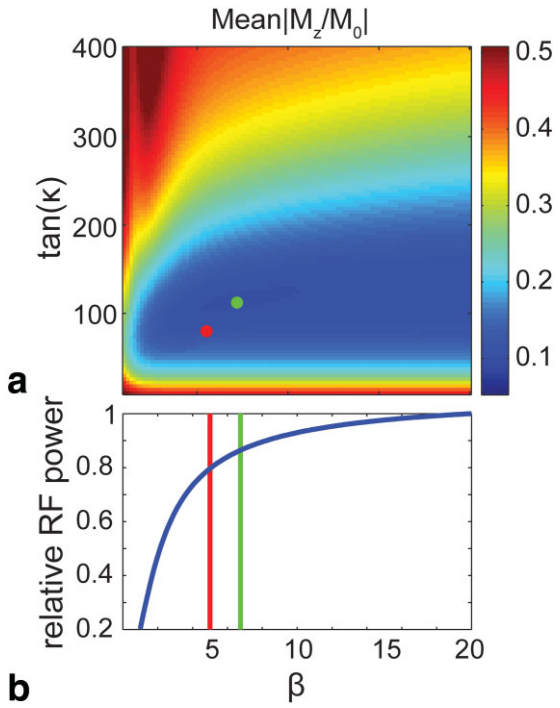

FIG. 5. Optimization of BIR-4 amplitude and frequency modulation function parameters β and tan(κ). Simulations show **(a)** mean ($\lvert M_z\rvert/M_0$) over the ROI as a function of β and tan(κ), and **(b)** relative RF power, which is a function of β only. The red dot (relative RF power = 0.80; β = 5; tanh(K) = 80) indicates the pulse used in this study, and the green dot (relative RF power = 0.86; β = 6.8; tanh(K) = 112) indicates the pulse with the lowest residual magnetization. [Color figure can be viewed in the online issue, which is available at www.interscience.wiley.com.]

First-pass contrast agents also cause a reduction in T_1 relaxation time, and longitudinal recovery during saturation may affect pulse performance. Fig. 6 shows the results of a numerical simulation of the residual $\lvert M_z/M_0\rvert$ within the ROI with different T_1 relaxation times (50–2000 msec). The BIR-4 pulse showed the least T_1 dependency with <2% variation for all cases (max $\lvert M_z/M_0\rvert$, mean $\lvert M_z/M_0\rvert$, and SD M_z/M_0), but the tailored pulse train also maintained comparable saturation performance in the short T_1 regime. Based on the robustness to off-resonance and T_1 dependency, we would expect the proposed saturation pulse to maintain its performance under the conditions of dynamic contrast-enhanced MRI.

The B_1 scale range in the ROI (0.38–1.2) overestimates the actual B_1 behavior of each subject because the individual B_1 distribution never spans the entire B_1 scale range. This can be partially attributed to errors in the transmit gain calibration and, specifically, the fact that transmit gain is typically calibrated based on a signal from an entire slice or prescribed volume. Similar to localized shimming and localized center frequency adjustment, the localized calibration of the transmit gain specifically to the heart would be desirable to produce a more accurate and tighter expected B_1 scale range.

The proposed pulse designs can also be applied to other areas of the body such as the abdomen. Tailored pulse trains should be optimized with respect to the B_0–B_1 ROI of each application, which in the abdomen could include fat.

In conclusion, we have described and experimentally validated the use of tailored pulse trains that optimally saturate myocardium at 3 T, based on measurements of typical B_0 and B_1 field variation. Weighted hard pulse trains are simple to design, require substantially lower RF power compared with BIR-4 pulses, and show higher B_1 insensitivity compared with conventional hard pulse trains. Furthermore, the proposed saturation pulse demonstrated lower peak and average residual M_z/M_0 over the heart at 3 T, compared with a standard 8-msec BIR-4 pulse and a conventional hard pulse train ($P < 0.05$). Tailored pulse trains may therefore have an important beneficial role in quantitative first-pass myocardial perfusion imaging at 3 T.

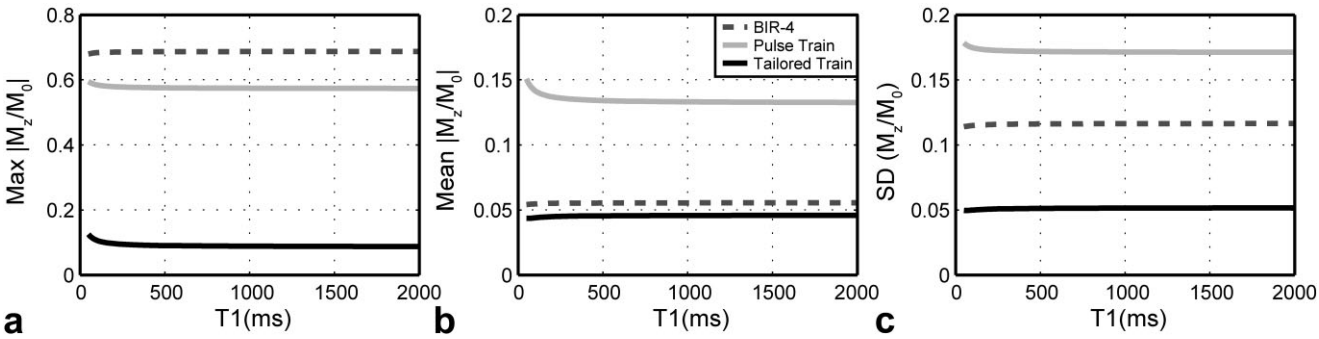

FIG. 6. The saturation effectiveness as a function of T_1-relaxation times. **(a)** Max $|M_z/M_0|$, **(b)** mean $|M_z/M_0|$, and **(c)** SD M_z/M_0 were simulated for the BIR-4 pulse (dotted line), pulse train (gray line), and tailored pulse train (black line).

REFERENCES

1. McNamara MT, Higgins CB, Ehman RL, Revel D, Sievers R, Brasch RC. Acute myocardial ischemia: magnetic resonance contrast enhancement with gadolinium-DTPA. Radiology 1984;153:157–163.
2. Atkinson DJ, Burstein D, Edelman RR. First-pass cardiac perfusion: evaluation with ultrafast MR imaging. Radiology 1990;174:757–762.
3. Schwitter J, Wacker CM, van Rossum AC, Lombardi M, Al-Saadi N, Ahlstrom H, Dill T, Larsson HBW, Flamm SD, Marquardt M, Johansson L. MR-IMPACT: comparison of perfusion-cardiac magnetic resonance with single-photon emission computed tomography for the detection of coronary artery disease in a multicentre, multivendor, randomised trial. Eur Heart J 2008;29:480–489.
4. Cheng ASH, Pegg TJ, Karamitsos TD, Searle N, Jerosch-Herold M, Choudhury RP, Banning AP, Neubauer S, Robson MD, Selvanayagam JB. Cardiovascular magnetic resonance perfusion imaging at 3 Tesla for the detection of coronary artery disease a comparison with 1.5-Tesla. J Am Coll Cardiol 2007;49:2440–2449.
5. Noeske R, Seifert F, Rhein KH, Rinneberg H. Human cardiac imaging at 3 T using phased array coils. Magn Reson Med 2000;44:978–982.
6. Singerman RW, Denison TJ, Wen H, Balaban RS. Simulation of B1 field distribution and intrinsic signal-to-noise in cardiac MRI as a function of static magnetic field. J Magn Reson 1997;125:72–83.
7. Wen H, Denison TJ, Singerman RW, Balaban RS. The intrinsic signal-to-noise ratio in human cardiac imaging at 1.5, 3, and 4 T. J Magn Reson 1997;125:65–71.
8. Greenman RL, Shirosky JE, Mulkern RV, Rofsky NM. Double inversion black-blood fast spin-echo imaging of the human heart: a comparison between 1.5T and 3.0T. J Magn Reson Imaging 2003;17:648–655.
9. Sung K, Nayak KS. Measurement and characterization of RF nonuniformity over the heart at 3T using body coil transmission. J Magn Reson Imaging 2008;27:643–648.
10. Oesingmann N, Zhang Q, Simonetti O. Improved saturation RF pulse design for myocardial first-pass perfusion at 3T. J Cardiovasc Magn Reson 2004;6:373–374.
11. Staewen RS, Johnson AJ, Ross BD, Parrish T, Merkle H, Garwood M. 3-D FLASH imaging using a single surface coil and a new adiabatic pulse, BIR-4. Invest Radiol 1990;25:559–567.
12. Kim D, Cernicanu A, Axel L. B(0) and B(1)-insensitive uniform T(1)-weighting for quantitative, first-pass myocardial perfusion magnetic resonance imaging. Magn Reson Med 2005;54:1423–1429.
13. Kim D, Gonen O, Oesingmann N, Axel L. Comparison of the effectiveness of saturation pulses in the heart at 3 T. Magn Reson Med 2008; 59:209–215.
14. Kino A, Zuehlsdorff S, Weale P, Leloudas N, Liu X, Jerecic R, Carr JC. Comparison of different field insensitive saturation pulses for 3T cardiac first pass perfusion. In: Proceedings of the 15th annual meeting of ISMRM, Berlin, 2007, p 2532.
15. Kellman P, Arai AE. Imaging sequences for first pass perfusion—a review. J Cardiovasc Magn Reson 2007;9:525–537.
16. Ogg RJ, Kingsley PB, Taylor JS. WET, a T1- and B1-insensitive water-suppression method for in vivo localized 1H NMR spectroscopy. J Magn Reson B 1994;104:1–10.
17. Stollberger R, Wach P. Imaging of the active B_1 field in vivo. Magn Reson Med 1996;35:246–251.
18. Cunningham CH, Pauly JM, Nayak KS. Saturated double-angle method for rapid B_1+ mapping. Magn Reson Med 2006;55:1326–1333.
19. Everitt BS, Hand DJ. Finite mixture distributions. New York: Chapman and Hall; 1981.
20. Edelman RR, Storey P, Dunkle E, Li W, Carrillo A, Vu A, Carroll TJ. Gadolinium-enhanced off-resonance contrast angiography. Magn Reson Med 2007;57:475–484.